Acta Crystallographica Section B
Structural Science
ISSN 0108-7681

Structural trends and the electronic structure of the rare-earth oxomolybdates RMo_5O_8 (R = La, Ce, Pr, Nd, Sm, Eu and Gd) containing chains of bioctahedral Mo_{10} clusters

P. Gougeon,[a]* P. Gall,[b] J.-F. Halet[a] and R. Gautier[c]

[a]Laboratoire de Chimie du Solide et Inorganique Moléculaire, UMR CNRS No. 6511, Université de Rennes 1, Institut de Chimie de Rennes, Avenue du Général Leclerc, 35042 Rennes CEDEX, France, [b]Laboratoire de Chimie des Matériaux Inorganiques et de Cristallographie, 20 avenue des buttes de Cöesmes, 35043 Rennes CEDEX, France, and [c]Département de Physicochimie UPRES 1795, Ecole Nationale Supérieure de Chimie de Rennes, Institut de Chimie de Rennes, Campus de Beaulieu, 35700 Rennes CEDEX, France

Correspondence e-mail: patrick.gougeon@univ-rennes1.fr

Received 19 March 2003
Accepted 9 May 2003

The crystal structures of the rare-earth members of the series RMo_5O_8 (R = Ce to Eu) have been investigated and compared with those of the La and Gd members previously published in order to understand the influences of the size and the charge of the cation on the different Mo—Mo bonds. The RMo_5O_8 compounds crystallize in the monoclinic space group $P2_1/c$. Their crystal structure is characterized by bioctahedral Mo_{10} clusters forming extended chains. The results of our single-crystal studies show that the modification of charge predominantly affects the Mo—Mo bonds between the Mo_{10} clusters and, to a lesser extent, the intra-cluster distances, while the cationic size induces only small variations. Theoretical investigations confirm this statement and allow the understanding of the bonding mode in these compounds.

1. Introduction

Among the reduced molybdenum oxides, the AMo_5O_8 compounds, which contain chains of bioctahedral Mo_{10} clusters running all along the crystal, have been the subject of electrical resistivity and magnetic studies (Gall *et al.*, 1993, 1995) because of the possibility of modifying the number of electrons available for metal–metal bonding in the cluster chains [often called metal electron (ME) count] without significantly altering the basic structure. In the case where the A cation is divalent (Ca, Sr, Eu) the AMo_5O_8 compounds are semiconducting in the 20–300 K range, whereas when A is trivalent (La, Ce, Pr, Nd or Sm) they show anomalous semiconductor-to-metal transitions near 180 K, followed by a re-entrant behavior to the semiconducting state between 30 and 50 K (Gall *et al.*, 1995). Recent work on the solid solution $Sr_{1-x}La_xMo_5O_8$ (x = 0–1) showed that when a small percentage of either La or Sr atoms is present, the $Sr_{1-x}La_xMo_5O_8$ compounds become metallic (McCarroll *et al.*, 1998). For a full understanding of the influence of the size and charge of the cation on the different Mo—Mo and Mo—O bonds in that structure type, we performed a complete structural study of the rare-earth members of the AMo_5O_8 family. In this paper these structural results are presented and discussed in correlation with quantum mechanical calculations that were performed using the extended Hückel method.

2. Experimental

2.1. Crystal growth

Single crystals of the rare-earth pentamolybdate RMo_5O_8 (R = Ce, Pr, Nd, Sm and Eu) were prepared from a stoichiometric mixture of MoO_3 (Strem Chemicals, 99.9%), Mo (Cime bocuze, 99.9%) and R_2O_3 for R = Nd and Sm (Strem

Table 1
Experimental data.

	$CeMo_5O_8$	$PrMo_5O_8$	$NdMo_5O_8$	$SmMo_5O_8$	$EuMo_5O_8$
Crystal data					
Chemical formula	$CeMo_5O_8$	$PrMo_5O_8$	$NdMo_5O_8$	$SmMo_5O_8$	$EuMo_5O_8$
M_r	747.82	748.61	751.94	758.05	759.66
Cell setting, space group	Monoclinic, $P2_1/c$	Monoclinic, $P2_1/c$	Monoclinic, $P2_1/c$	Monoclinic, $P2_1/c$	Monoclinic, $P2_1/c$
a, b, c (Å)	7.5643 (1), 9.0693 (1), 9.9150 (2)	7.5662 (1), 9.0569 (1), 9.9175 (1)	7.5606 (1), 9.0392 (1), 9.9082 (2)	7.5620 (2), 9.0197 (2), 9.9226 (2)	7.5554 (1), 9.1622 (2), 9.9685 (2)
α, β, γ (°)	90.00, 109.2113 (8), 90.00	90.00, 109.3293 (7), 90.00	90.00, 109.4513 (7), 90.00	90.00, 109.6643 (12), 90.00	90.00, 109.3560 (9), 90.00
V (Å^3)	642.32 (2)	641.30 (1)	638.50 (2)	637.32 (3)	651.06 (2)
Z	4	4	4	4	4
D_x (Mg m^{-3})	7.733	7.754	7.822	7.900	7.750
Radiation type	Mo $K\alpha$	Mo $K\alpha$	Mo $K\alpha$	Mo $K\alpha$	Mo $K\alpha$
No. of reflections for cell parameters	9841	11 309	12 284	6858	12 022
θ range (°)	1–37.8	1.0–37.8	1.0–37.8	2.9–37.8	1.0–37.8
μ (mm^{-1})	16.42	16.94	17.52	18.61	18.84
Temperature (K)	293 (2)	293 (2)	293 (2)	293 (2)	293 (2)
Crystal form, colour	Plate, black	Irregular plate, black	Irregular plate, black	Irregular plate, black	Irregular plate, black
Crystal size (mm)	0.14 × 0.10 × 0.08	0.24 × 0.11 × 0.04	0.13 × 0.13 × 0.08	0.09 × 0.06 × 0.03	0.10 × 0.07 × 0.05
Data collection					
Diffractometer	Nonius KappaCCD	Nonius KappaCCD	Nonius KappaCCD	Nonius KappaCCD	Nonius KappaCCD
Data collection method	ϕ scans ($\kappa = 0$) + additional ω scans	ϕ scans ($\kappa = 0$) + additional ω scans	ϕ scans ($\kappa = 0$) + additional ω scans	ϕ scans ($\kappa = 0$) + additional ω scans	ϕ scans ($\kappa = 0$) + additional ω scans
Absorption correction	Gaussian	Gaussian	Multi-scan (based on symmetry-related measurements)	Multi-scan (based on symmetry-related measurements)	Multi-scan (based on symmetry-related measurements)
T_{min}	0.064	0.090	0.113	0.378	0.168
T_{max}	0.181	0.524	0.252	0.513	0.358
No. of measured, independent and observed reflections	12 944, 3402, 3314	14 762, 3411, 3329	17 433, 3404, 3193	15 935, 3395, 2569	6545, 3471, 3034
Criterion for observed reflections	$I > 2\sigma(I)$	$I > 2\sigma(I)$	$I > 2\sigma(I)$	$I > 2\sigma(I)$	$I > 2\sigma(I)$
R_{int}	0.064	0.091	0.052	0.075	0.031
θ_{max} (°)	37.8	37.8	37.8	37.8	37.8
Range of h, k, l	$-12 \Rightarrow h \Rightarrow 11$ $-15 \Rightarrow k \Rightarrow 15$ $-12 \Rightarrow l \Rightarrow 17$	$-12 \Rightarrow h \Rightarrow 12$ $-15 \Rightarrow k \Rightarrow 15$ $-16 \Rightarrow l \Rightarrow 16$	$-12 \Rightarrow h \Rightarrow 12$ $-15 \Rightarrow k \Rightarrow 15$ $-14 \Rightarrow l \Rightarrow 16$	$-12 \Rightarrow h \Rightarrow 13$ $-15 \Rightarrow k \Rightarrow 15$ $-17 \Rightarrow l \Rightarrow 15$	$0 \Rightarrow h \Rightarrow 13$ $0 \Rightarrow k \Rightarrow 15$ $-16 \Rightarrow l \Rightarrow 16$
Refinement					
Refinement on	F^2	F^2	F^2	F^2	F^2
$R[F^2 > 2\sigma(F^2)]$, $wR(F^2)$, S	0.034, 0.080, 1.26	0.029, 0.070, 1.19	0.024, 0.055, 1.16	0.039, 0.087, 1.03	0.032, 0.077, 1.06
No. of relections	3402	3411	3404	3395	3471
No. of parameters	128	128	128	128	128
Weighting scheme	$w = 1/[\sigma^2(F_o^2) + (P)^2 + 7.228P]$, where $P = (F_o^2 + 2F_c^2)/3$	$w = 1/[\sigma^2(^oF2) + (0.0145P)^2 + 1.922P]$, where $P = (F_o^2 + 2F_c^2)/3$	$w = 1/[\sigma^2(F_o^2) + (P)^2 + 2.8951P]$, where $P = (F_o^2 + 2F_c^2)/3$	$w = 1/[\sigma^2(F_o^2) + (0.0313P)^2]$, where $P = (F_o^2 + 2F_c^2)/3$	$w = 1/[\sigma^2(F_o^2) + (0.0324P)^2 + 2.9295P]$, where $P = (F_o^2 + 2F_c^2)/3$
$(\Delta/\sigma)_{max}$	0.001	0.002	0.001	0.001	0.001
$\Delta\rho_{max}$, $\Delta\rho_{min}$ (e Å^{-3})	2.54, −2.50	2.45, −3.32	1.63, −1.82	4.49, −2.89	3.59, −4.08
Extinction method	*SHELXL*	*SHELXL*	*SHELXL*	*SHELXL*	*SHELXL*
Extinction coefficient	0.0171 (5)	0.0874 (12)	0.0185 (3)	0.00439 (19)	0.0189 (4)

Computer programs: *COLLECT* (Nonius, 1998), *DENZO and SCALEPACK* (Otwinowski & Minor, 1997), *SHELXL*97 (Sheldrick, 1997), *DIAMOND* (Bergerhoff, 1996).

Chemicals, 99.999%). For the Ce and Pr compounds, the starting rare-earth oxides were CeO_2 (Strem Chemicals, 99.999%) and Pr_6O_{11} (Strem Chemicals, 99.9%). Before use the Mo powder was reduced under a hydrogen flow at 1273 K for 6 h and the rare-earth oxides were prefired at temperatures between 973 and 1273 K overnight and left at 873 K before weighing. The stoichiometric mixtures were pressed into *ca* 5 g pellets, loaded into molybdenum crucibles (depth: 2.5 cm; diameter: 1.5 cm), which were previously cleaned by heating at 1773 K for 15 min under a dynamic vacuum of *ca* 10^{-5} Torr, and then sealed under low argon pressure using an arc-welding system. The charges were heated at a rate of 300 K h^{-1} to 1973 K for 5 min and then cooled at 50 K h^{-1} to 1373 K, at which point the furnace was shut down and allowed to cool to room temperature. The crystals were generally obtained as thin black truncated plates.

2.2. Single-crystal X-ray diffraction studies

Intensity data were collected on a Nonius Kappa CCD diffractometer using graphite-monochromated Mo $K\alpha$ radiation (λ = 0.71073 Å) at room temperature. The frames were recorded using $\Delta\omega = 2^\circ$ rotation scans with X-ray exposure times of 20 or 40 s. Reflection indexing, a Lorentz–polarization correction, peak integration and background determination were performed using the programs *DENZO* and *SCALEPACK* (Otwinowski & Minor, 1997) of the Kappa CCD software package (Nonius, 1998). All structures were refined in the monoclinic space group $P2_1/c$ using *SHELXL*97 (Sheldrick, 1997). Positional parameters of $LaMo_5O_8$ (Hibble *et al.*, 1988) were used in the first stages of the refinements. The final refinement cycles included the atomic coordinates and anisotropic displacement parameters for all atoms. Refinement of the occupancy factor of the rare-earth site showed that it is fully occupied in all the crystals investigated. The details of the X-ray single data collections and structure refinements for the RMo_5O_8 compounds are summarized in Table 1.[1] Selected interatomic distances are given in Table 2 and compared with those observed in the previously published compounds $LaMo_5O_8$ (Gall & Gougeon, 1994*b*) and $GdMo_5O_8$ (Gougeon *et al.*, 1991).

Table 2
Selected bond distances (Å) for RMo_5O_8.

	La	Ce	Pr	Nd	Sm	Eu	Gd
R—O1^{i}	2.442 (3)	2.410 (3)	2.397 (2)	2.379 (2)	2.355 (3)	2.535 (3)	2.315 (5)
R—O1^{ii}	2.459 (3)	2.443 (3)	2.423 (2)	2.406 (2)	2.384 (4)	2.545 (3)	2.364 (5)
R—O4^{iii}	2.487 (3)	2.459 (3)	2.440 (2)	2.425 (2)	2.398 (4)	2.596 (3)	2.387 (5)
R—O7^{ii}	2.574 (3)	2.568 (3)	2.550 (2)	2.540 (2)	2.517 (3)	2.657 (3)	2.506 (5)
R—O5^{iv}	2.675 (4)	2.648 (3)	2.632 (2)	2.614 (2)	2.584 (3)	2.715 (3)	2.556 (5)
R—O3^{v}	2.731 (3)	2.709 (3)	2.697 (2)	2.676 (2)	2.652 (3)	2.744 (3)	2.634 (5)
R—O8^{iii}	2.703 (3)	2.713 (3)	2.721 (2)	2.725 (2)	2.748 (3)	2.751 (3)	2.779 (5)
R—O2^{i}	2.763 (3)	2.758 (3)	2.757 (2)	2.752 (2)	2.750 (3)	2.771 (3)	2.739 (5)
R—O6^{iii}	2.806 (4)	2.862 (3)	2.868 (2)	2.867 (2)	2.894 (3)	2.932 (3)	2.905 (5)
R—O2^{vi}	2.919 (3)	2.930 (3)	2.933 (2)	2.936 (2)	2.947 (3)	2.947 (3)	2.959 (5)
Mo1—Mo2^{vii}	2.6816 (5)	2.6874 (7)	2.6867 (3)	2.6847 (4)	2.6876 (5)	2.6947 (4)	2.682 (1)
Mo1—Mo4	2.7876 (5)	2.7906 (5)	2.7937 (3)	2.7923 (4)	2.7964 (5)	2.7549 (4)	2.795 (1)
Mo1—Mo5^{viii}	2.8094 (5)	2.8086 (5)	2.8094 (3)	2.8070 (3)	2.8073 (6)	2.7678 (4)	2.807 (1)
Mo1—Mo3^{vii}	2.8124 (5)	2.8111 (5)	2.8116 (3)	2.8085 (4)	2.8077 (5)	2.7749 (4)	2.802 (1)
Mo1—Mo1^{vii}†	2.6890 (7)	2.6851 (5)	2.6855 (4)	2.6822 (5)	2.6818 (8)	2.7670 (6)	2.674 (1)
Mo1—Mo2†	2.9108 (5)	2.9066 (5)	2.9058 (3)	2.9035 (4)	2.9050 (6)	3.0366 (4)	2.904 (1)
Mo1—Mo3†	3.0911 (5)	3.0840 (5)	3.0845 (3)	3.0815 (4)	3.0787 (6)	3.0869 (5)	3.078 (1)
Mo2—Mo4^{vii}	2.7288 (5)	2.7279 (5)	2.7275 (3)	2.7253 (4)	2.7249 (6)	2.7420 (4)	2.722 (1)
Mo2—Mo5	2.7609 (5)	2.7579 (5)	2.7579 (3)	2.7546 (4)	2.7527 (6)	2.7218 (4)	2.750 (1)
Mo2—Mo3	2.8279 (5)	2.8282 (5)	2.8300 (3)	2.8276 (4)	2.8309 (6)	2.8286 (4)	2.832 (1)
Mo3—Mo4^{ix}	2.6102 (5)	2.6072 (5)	2.6057 (3)	2.6028 (4)	2.6020 (6)	2.6067 (4)	2.598 (1)
Mo3—Mo5^{x}	2.6727 (5)	2.6726 (5)	2.6731 (3)	2.6715 (4)	2.6727 (6)	2.6951 (4)	2.669 (1)
Mo3—Mo5	2.7558 (5)	2.7569 (5)	2.7591 (3)	2.7585 (4)	2.7647 (5)	2.7529 (4)	2.765 (1)
Mo4—Mo5^{viii}	2.7505 (5)	2.7474 (5)	2.7458 (3)	2.7413 (4)	2.7393 (5)	2.7430 (4)	2.735 (1)
Mo4—Mo5^{vii}	2.7605 (5)	2.7594 (5)	2.7599 (3)	2.7584 (4)	2.7580 (6)	2.7720 (4)	2.757 (1)
Mo5—Mo5^{x}	2.8172 (7)	2.8183 (6)	2.8201 (4)	2.8192 (5)	2.8215 (7)	2.8327 (6)	2.822 (1)

Symmetry codes: (i) $-x+1, y+\frac{1}{2}, -z+\frac{3}{2}$; (ii) $x, -y+\frac{1}{2}, z-\frac{1}{2}$; (iii) $x, -y+\frac{1}{2}, z+\frac{1}{2}$; (iv) $-x+1, y+\frac{1}{2}, -z+\frac{1}{2}$; (v) $-x, y+\frac{1}{2}, -z+\frac{1}{2}$; (vi) $-x, y+\frac{1}{2}, -z+\frac{3}{2}$; (vii) $-x+1, -y, -z+1$; (viii) $x+1, y, z$; (ix) $x, y-1, z$; (x) $x-1, y, z$. † Intercluster distance.

3. Results and discussion

3.1. Structural aspect

The structural type $LaMo_5O_8$ was first described by Hibble *et al.* in 1988 (Hibble *et al.*, 1988). The structure was determined from X-ray and neutron powder-diffraction data and subsequently by various authors from single-crystal data for other cations such as Sn (Gougeon *et al.*, 1990), Pb (Dronskowski & Simon, 1989; Dronskowski *et al.*, 1991), La (Gall & Gougeon, 1994*a*), Gd (Gougeon *et al.*, 1991) and Sr (Gall & Gougeon, 1994*a*). The basic structural building block is the bioctahedral cluster unit $[Mo_{10}O^{i}_{18}][O^{a}_{8}$, which results from the metal edge condensation of two $[Mo_6O^{i}_{12}][O^{a}_{6}$ -type clusters (Fig. 1). The $[Mo_{10}O^{i}_{18}][O^{a}_{8}$ cluster units are linked on opposite edges *via* common O atoms to form chains extended all along the crystal, the connectivity formula of which is $[Mo_{10}O^{i}_{12}O^{i-i}_{4/2}O^{i-a}_{2/2}][O^{a}_{6}O^{a-i}_{2/2}$ (Fig. 2). Within these chains, the Mo_{10} clusters are bonded through one short intercluster Mo1—Mo1 bond and two weaker Mo1—Mo2 bonds (Fig. 3). Two long intercluster Mo1—Mo3 bonds are also observed. These chains which run parallel to the *a* axis then share the remaining O^{a} atoms to create one-dimensional channels which can accommodate a large variety of cations (Fig. 4). The latter can be divalent (Ca, Sr, Sn, Pb or Eu) or trivalent (La–Sm and Gd). As a consequence, the MMo_5O_8 compounds are described by the following connective formula, $(M^{x+})_2$ $([Mo_{10}O^{i}_{6}O^{i-i}_{4/2}O^{i-a}_{8/2}][O^{a-i}_{8/2})^{2x-}$ $(2 \leq x \leq 3)$.

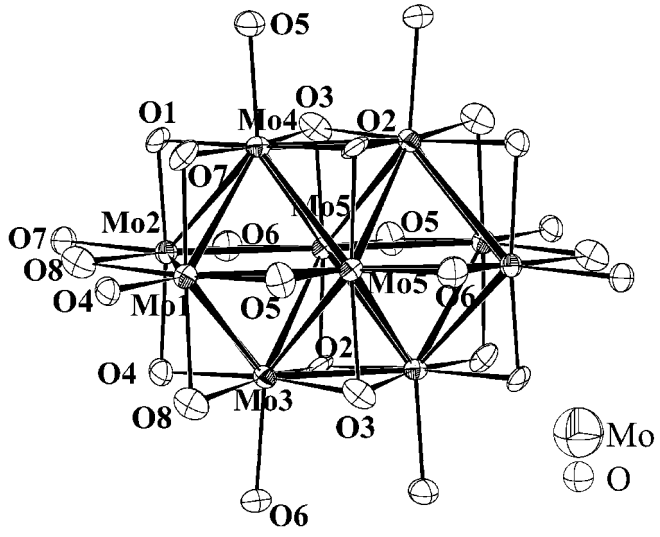

Figure 1
The bioctahedral $[Mo_{10}O^{i}_{18}][O^{a}_{8}$ cluster unit with the numbering scheme used in the RMo_5O_8 compounds.

[1] Supplementary data for this paper are available from the IUCr electronic archives (Reference: NA5000). Services for accessing these data are described at the back of the journal.

The rare-earth members of the AMo_5O_8 series provide a favorable system to study the influence of the size of the cation and that of its charge on the different Mo—Mo and Mo—O bonds in that structure type. Fig. 5 shows the variation of the unit-cell volume as a function of the cube of the ionic radius. For the $R^{3+}Mo_5O_8$ compounds with R = La–Sm and Gd, we observe a linear decrease of the unit-cell volume from La to Gd, in agreement with the lanthanide contraction. The larger unit-cell volume (similar to that of the strontium analog) of the europium compound clearly indicates that the europium is in the divalent state, while the other rare earths are trivalent. This has also been confirmed by magnetic susceptibility measurements, which have lead to a magnetic moment of 7.77 μ_β, in good agreement with the free-ion value of divalent europium (μ_{th} = 7.94 μ_β).

3.1.1. Mo—Mo bonds. Fig. 6 shows the different Mo—Mo distances within the Mo_{10} cluster against the rare-earth ionic radius. The latter was taken as the difference between the average R—O distances and the ionic radius of O^{2-}. Examination of these plots reveals that the increase in the rare-earth ionic radius only induces small quasi-linear variations (maximum difference of 0.016 Å for the Mo1—Mo1 and Mo4—Mo5 bonds) on the intra- and intercluster distances for the RMo_5O_8 compounds containing a trivalent rare earth (R = La–Sm and Gd). On the other hand, the different Mo—Mo distances in the europium analog do not follow the general trend observed for the RMo_5O_8 compounds. Indeed, most of the Mo—Mo distances in $EuMo_5O_8$ have values which are not commensurate with the average ionic radius of the rare-earth site. For instance, the Mo1—Mo3, Mo1—Mo4, Mo1—Mo5, Mo2—Mo5, Mo3—Mo4 and Mo4—Mo5 (represented by thick lines in Fig. 3) distances are smaller by *ca* 0.03–0.06 Å than the values extrapolated from the linear laws followed by the Mo—Mo distances when the rare earth is trivalent, whereas the Mo1—Mo2, Mo2—Mo3, Mo2—Mo4, Mo3—Mo5, Mo4—Mo5 and Mo5—Mo5 (thin lines in Fig. 3) distances are slightly larger by *ca* 0.01 to 0.02 Å. The difference in behavior between the $R^{3+}Mo_5O_8$ compounds and $Eu^{2+}Mo_5O_8$ results principally from the diminution of the cationic charge transfer towards

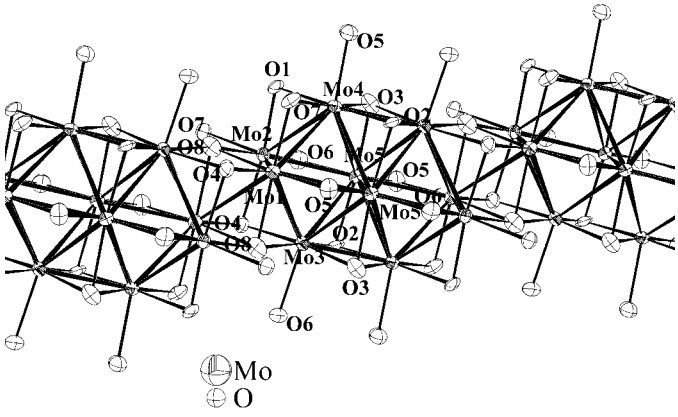

Figure 2
Fragment of the extented chain in the RMo_5O_8 compounds.

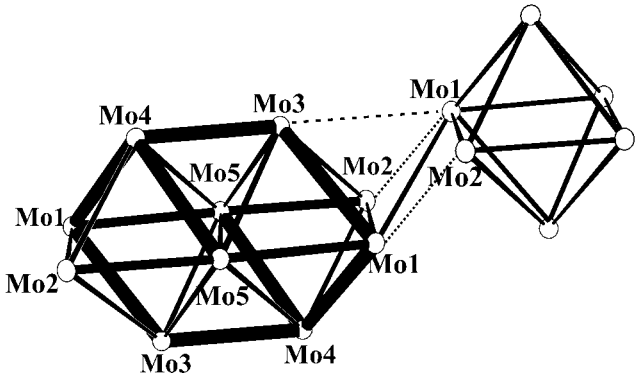

Figure 3
Detail of the interconnection between the Mo_{10} clusters in the RMo_5O_8 compounds. See text for the explanation about the thin and thick lines.

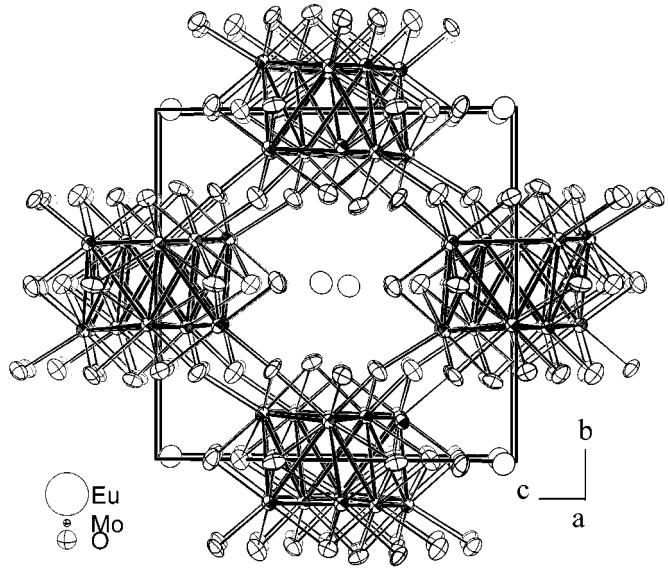

Figure 4
Projection of the crystal structure of RMo_5O_8 along the monoclinic a axis showing the interchain linkage.

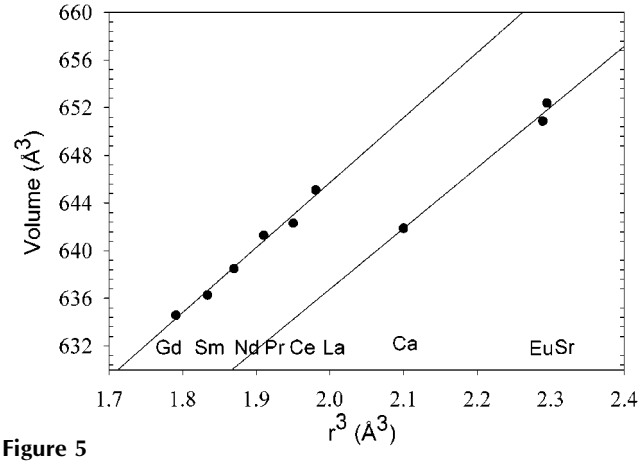

Figure 5
Variation of the unit-cell volume as a function of the cube of the ionic radius of the cation.

the Mo network in the Eu compound. This electronic effect is particularly important for the two intercluster Mo1—Mo1 and Mo1—Mo2 distances. These distances deviate by *ca* 0.08 and 0.12 Å, respectively, from the values expected from the fit of the curve *d*(Mo—Mo) *versus* the rare-earth ionic radius. This behavior is followed by the $R^{3+}Mo_5O_8$ compounds (Fig. 7). This curve clearly suggests that the extra electrons brought by the trivalent cations are principally included in these two intercluster bonds. On the other hand, one can also notice that the electronic effect is also very sensitive, as illustrated by the two compounds $Sr_{0.90}La_{0.10}Mo_5O_8$ and $Sr_{0.11}La_{0.89}Mo_5O_8$ of the solid solution between $SrMo_5O_8$ and $LaMo_5O_8$, which both differ only by *ca* 0.2 e^- per Mo_{10} cluster from the end members.

Within the Mo_{10} cluster, the overall effect of the reduction of the cationic charge transfer is a slight diminution of the average Mo—Mo distance from 2.7483 (1) Å when the cation is trivalent to 2.7417 (1) Å for divalent europium. For $Sr_{0.90}La_{0.10}Mo_5O_8$ and $Sr_{0.11}La_{0.89}Mo_5O_8$ the mean values are 2.7420 (1) and 2.7467 (1) Å, respectively, in agreement with the progressive augmentation of the cationic charge transfer towards the bioctahedral Mo_{10} cluster.

3.1.2. Mo—O distances. The various Mo—O distances show no well defined variations with respect to the ionic radii of the cations in the compounds containing trivalent rare earths and range from 1.990 to 2.146 Å, with mean values of 2.0755 (6), 2.0756 (6), 2.0764 (4), 2.0756 (4), 2.0765 (6) and 2.0747 (6) Å for the La, Ce, Pr, Nd, Sm and Gd compounds, respectively. On the other hand, the effect of the charge transfer is particularly important for the Mo2—O6 bond, which increases by *ca* 0.08 Å when the charge increases by 2 e^- per Mo_{10} cluster ($EuMo_5O_8$ to $LaMo_5O_8$). The general trend of the Mo—O bonds is an increase in length with increasing charge of the cations, as reflected by the average Mo—O bond which is 2.0639 (6) Å in $EuMo_5O_8$ and 2.0758 (2) Å in the RMo_5O_8 compounds containing trivalent cations. This trend is confirmed by $Sr_{0.90}La_{0.10}Mo_5O_8$ and $Sr_{0.11}La_{0.89}Mo_5O_8$, in which the mean values are 2.0657 (6) and 2.0748 (4) Å, respectively.

3.1.3. *R*—O distances. The variations in the *R*—O distances as a function of the ionic radius of the rare earths is shown in Fig. 8. For the $R^{3+}Mo_5O_8$ compounds, the first seven *R*—O distances increase quasi-linearly when the rare-earth ionic radius increases. This indicates that these O atoms are the nearest neighbors of the rare earth. The remaining three *R*—O distances decrease when the rare-earth ionic radius increases, indicating that these three O atoms are second nearest neighbors. The larger rare-earth oxygen bond lengths observed in $EuMo_5O_8$ reflect the divalent state of the europium again.

3.2. Theoretical considerations

In order to understand the structural variations encountered in RMo_5O_8 compounds, electronic structure calculations were carried out on $EuMo_5O_8$ and $LaMo_5O_8$ using extended Hückel theory (EH; Hoffmann, 1963). Previous EH tight-binding (EHTB; Whangbo & Hoffmann, 1978) calculations

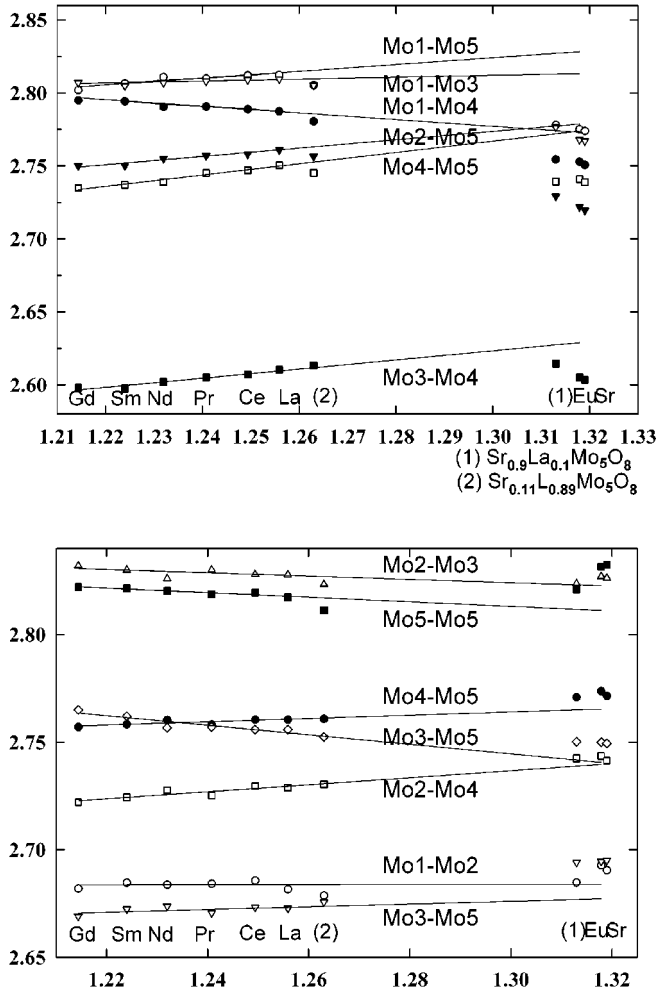

Figure 6
Variations of the Mo—Mo distances within the Mo_{10} cluster as a function of the crystal radius of the rare-earth cation.

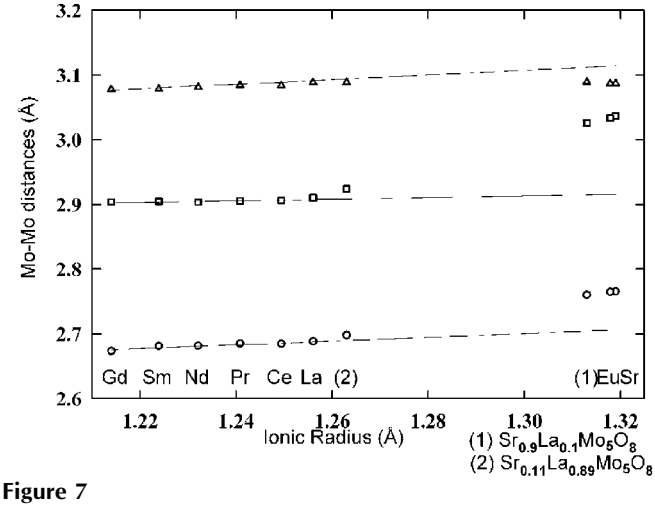

Figure 7
Variations of the intercluster Mo—Mo distances as a function of the crystal radius of the rare-earth cation. Triangles: Mo1—Mo3. Squares: Mo1—Mo2. Circles: Mo1—Mo1.

were carried out with the aim of understanding the physical properties of these compounds, especially the unusual electrical behavior of the trivalent cations in $R\mathrm{Mo_5O_8}$ compounds (Koo *et al.*, 1998). The theoretical analysis here is devoted to the study of the bonding properties of these materials.

Molecular and tight-binding calculations were carried out using the programs *CACAO* (Mealli & Proserpio, 1990) and *YaEHMOP* (Landrum, 1997), respectively. The exponents (ζ) and the valence-shell ionization potentials (H_{ii} in eV) were (respectively): 2.275, −32.3 for O 2*s*; 2.275, −14.8 for O 2*p*; 1.956, −8.34 for Mo 5*s*; 1.921, −5.24 for Mo 5*p*; 2.14. H_{ii} values for Mo 4*d* were set equal to −10.50. A linear combination of the two Slater-type orbitals of exponents $\zeta_1 = 4.542$ and $\zeta_2 = 1.901$, with equal weighting coefficients, was used to represent the Mo 4*d* atomic orbitals. The density of states (DOS) and crystal orbital overlap populations (COOP) of $\mathrm{EuMo_5O_8}$ and $\mathrm{LaMo_5O_8}$ were obtained using a set of 27 *k* points.

The metallic electron (ME) count per $\mathrm{Mo_{10}}$ motif in $R\mathrm{Mo_5O_8}$ compounds is equal to 32 and 34 for divalent and trivalent cations, respectively. Suprisingly, this is higher than the optimal ME count of 30 for isolated $\mathrm{Mo_{10}}$ clusters, which are present in $R_{16}\mathrm{Mo_{21}O_{56}}$ compounds (Gall *et al.*, 1999), in contrast to the general idea that the number of electrons of a system decreases when the connectivity increases. The study of a hypothetical $\mathrm{Mo_{20}O_{48}}$ dimer, built with two $\mathrm{Mo_{10}}$ units linked in the same manner as in $R\mathrm{Mo_5O_8}$ compounds, seems to be a good starting point for the bonding analysis in $\mathrm{Mo_5O_8}$ chains in order to detect which molecular orbitals (MO) of the $\mathrm{Mo_{10}}$ isolated units were involved in the inter-cluster bonding.

In $\mathrm{Mo_5O_8}$ chains the oxygen environment is the same as in isolated $\mathrm{Mo_{10}}$ clusters; the only difference is in the metallic environment of some metallic atoms. Metallic MOs of the isolated $\mathrm{Mo_{10}}$ units must be more perturbed than other MOs when considering inter-cluster interactions. EH calculations on the $\mathrm{Mo_{20}O_{48}}$ dimer model confirm this. The largest interaction occurs between the lowest unoccupied MOs (LUMOs) of the $\mathrm{Mo_{10}}$ units (see Fig. 9). These MOs are essentially localized on the Mo1 atoms and their orientation allows a σ-type overlap between clusters in the Mo1—Mo1 direction. The magnitude of the interaction is large enough so that the resulting in-phase combination is low enough to be occupied and is separated by a gap of 0.34 eV from the highest-energy MOs (see Fig. 9). This gap becomes the HOMO/LUMO gap for the ME count of 30 + 30 + 2 = 62. The Mo1—Mo1 inter-cluster overlap population is increased by 50% when the Mo1—Mo1 bonding MO is occupied and equal to 0.172; this value is quite large, indicating that inter-cluster bonding is of the same order of magnitude as intra-cluster bonding. Considering two electrons per inter-cluster contact, the optimal ME count per $\mathrm{Mo_{10}}$ cluster in the $\mathrm{Mo_5O_8}$ chain is 32, as observed in the divalent cation compounds. To a lesser extent, LUMOs for 62 MEs in the dimer model show some inter-cluster Mo—Mo bonding character. For larger electron counts (such as 34 ME per $\mathrm{Mo_{10}}$ motif, as observed in trivalent rare-earth compounds; 64 ME for the dimer model), the shortening of some Mo—Mo inter-cluster bonds is foreseen. An increase of the intra-cluster bonds in $R\mathrm{Mo_5O_8}$ compared with those of isolated $\mathrm{Mo_{10}}$ clusters in $\mathrm{R_{16}Mo_{21}O_{56}}$ compounds is explained by the occupation of these MOs, which assume inter-cluster bonds and present some antibonding intra-cluster Mo—Mo character.

In order to confirm these conclusions, EHTB DOS and COOP calculations were carried out on the $\mathrm{Mo_5O_8}$ network with $\mathrm{EuMo_5O_8}$ and $\mathrm{LaMo_5O_8}$ crystallographic structures (Fig. 10); the EHTB approximation allowing the treatment of Eu and La atoms as Eu^{2+} and La^{3+}, giving their valence electrons (2 and 3, respectively). DOS and COOP curves of $\mathrm{EuMo_5O_8}$ and $\mathrm{LaMo_5O_8}$ are very similar because of their

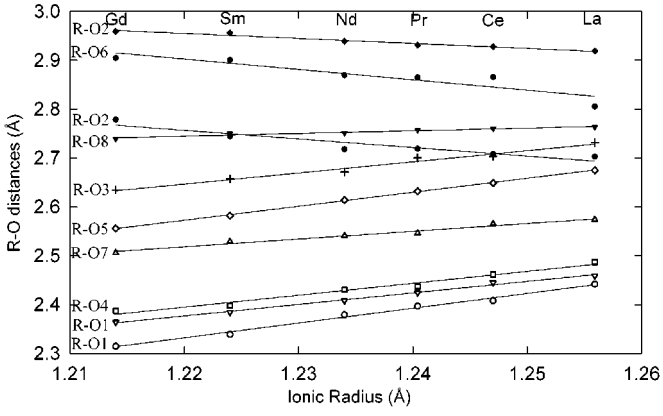

Figure 8
Variations of the *R*—O distances as a function of the crystal radius of the rare-earth cation.

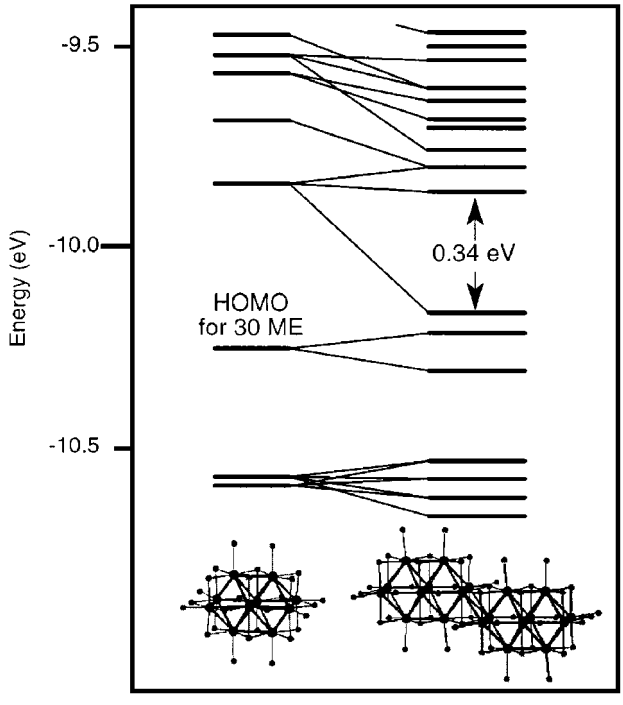

Figure 9
Correlation diagram relating molecular orbitals of the $\mathrm{Mo_{10}O_{26}}$ cluster to those of the $\mathrm{Mo_{20}O_{48}}$ dimer.

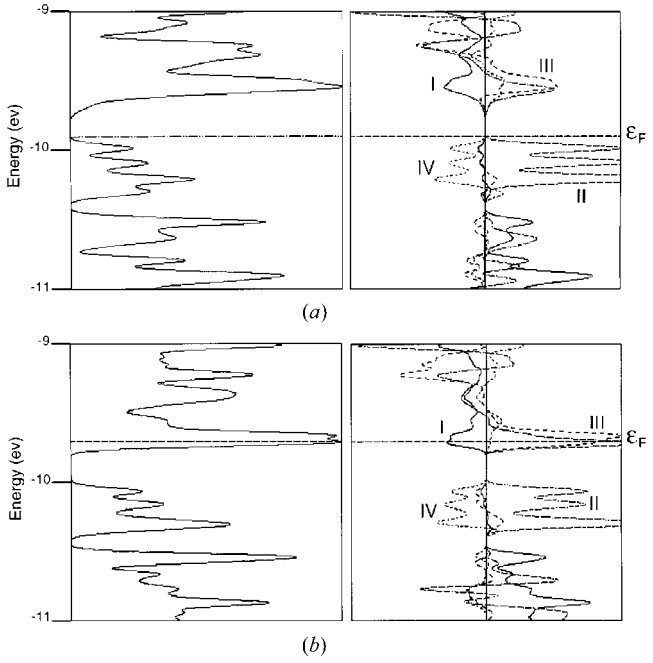

Figure 10
DOS and (I) Mo—Mo intra-cluster, (II) Mo1—Mo1 inter-cluster, (III) Mo1—Mo2 inter-cluster and (IV) Mo1—Mo3 COOP curves of (*a*) $EuMo_5O_8$ and (*b*) $LaMo_5O_8$.

rather small crystal structure differences. One can recognize the general features of the dimer model MO diagram: the Mo1—Mo1 bonding DOS peak below the small energetic gap and DOS peak with Mo1—Mo1 and Mo1—Mo2 bonding character just above it. For the RMo_5O_8 structure with trivalent ions, this latter DOS peak is partially occupied. The occupation of these states explains the shortening of the Mo1—Mo1 and Mo1—Mo2 distances by *ca* 0.1 Å. Mo—Mo inter-cluster overlap populations increase from 0.149 to 0.193 between Mo1 atoms, from 0.009 to 0.052 between Mo1 and Mo2 atoms, whereas Mo1—Mo3 overlap populations is still equal to 0. This indicates rather strong Mo1—Mo1 bonding in both divalent and trivalent compounds and significant Mo1—Mo2 bonding only in trivalent ones.

References

Bergerhoff, G. (1996). *DIAMOND*. Visual Crystal Structure Information System. University of Bonn, Germany.

Dronskowski, R. & Simon, A. (1989). *Angew. Chem. Int. Ed. Engl.* **28**, 758–760.

Dronskowski, R., Simon, A. & Mertin, W. (1991). *Z. Anorg. Allg. Chem.* **602**, 49–63.

Gall, P., Gautier, R., Halet, J.-F. & Gougeon, P. (1999). *Inorg. Chem.* **38**, 4455–4461.

Gall, P. & Gougeon, P. (1994*a*). *Acta Cryst.* C**50**, 7–9.

Gall, P. & Gougeon, P. (1994*b*). *Acta Cryst.* C**50**, 1183–1185.

Gall, P., Gougeon, P., Greenblatt, M., Jones, E. B., McCarroll, W. H. & Ramanujachary, K. V. (1995). *Croat. Chem. Acta*, **68**, 849.

Gall, P., Noël, H. & Gougeon, P. (1993). *Mater. Res. Bull.* **28**, 1225–1231.

Gougeon, P., Gall, P. & Sergent, M. (1991). *Acta Cryst.* C**47**, 421–423.

Gougeon, P., Potel, M. & Sergent, M. (1990). *Acta Cryst.* C**46**, 1188–1190.

Hibble, S. J., Cheetham, A. K., Bogle, A. R. L., Wakerley, H. R. & Cox, D. E. (1988). *J. Am. Chem. Soc.* **110**, 3295–3296.

Hoffmann, R. (1963). *J. Chem. Phys.* **39**, 1997.

Koo, H.-J., Whangbo, M.-H., McCarroll, W. H., Greenblatt, M., Gautier, R., Halet, J.-F. & Gougeon, P. (1998). *Solid State Commun.* **8**, 539–544.

Landrum, G. A. (1997). *YAeHMOP*. Version 2.0. Ithaca, New York, USA.

McCarroll, W. H., Borgia, M., Ramanujachary, K. V., Greenblatt, M., Gougeon, P. & Greedan, J. E. (1998). *J. Solid State Chem.* **138**, 7–17.

Mealli, C. & Proserpio, D. (1990). *J. Chem. Educ.* **67**, 399–402.

Nonius (1998). *Collect: KappaCCD Software.* Nonius BV, Delft, The Netherlands.

Otwinowski, Z. & Minor, W. (1997). *Methods in Enzymology*, edited by C.W. Carter Jr and R. M. Sweet, Vol. 276, pp. 307–326. New York: Academic Press.

Sheldrick, G. M. (1997). *SHELXL*97. University of Göttingen, Germany.

Whangbo, M.-H. & Hoffmann, R. (1978). *J. Am. Chem. Soc.* **100**, 6093.